Hyperspectral Image Segmentation and Clustering for Intraoperative Diagnosis of Intestinal Ischemia

Ilya Goryunov[1*], Valery Shupletsov[1], Nikita Adamenkov[1,2], Andrian Mamoshin[1,3], Elena Potapova[1], Andrey Dunaev[1] and Viktor Dremin[1,4]

[1] Orel State University named after I.S. Turgenev, Research and Development Center of Biomedical Photonics, 95 Komsomolskaya St., Orel 302026, Russian Federation

[2] Orel Regional Clinical Hospital, 10 Pobedy Blvd., Orel 302028, Russian Federation

[3] The National Medical Research Center of Surgery named after A. Vishnevsky, 27 Bolshaya Serpukhovskaya St., Moscow 117997, Russian Federation

[4] Aston Institute of Photonic Technologies, Aston University, Birmingham B4 7ET, United Kingdom

*e-mail: goryunow.il@yandex.ru

Abstract. We present an intraoperative hyperspectral imaging (HSI) approach for the assessment of intestinal ischemia, integrating deep learning-based segmentation with unsupervised spectral clustering. Sixteen patients were enrolled, of whom hyperspectral datasets from three representative cases were analyzed in detail. The developed convolutional neural network (1D-CNN) demonstrated high classification performance between intestinal tissue and background, enabling consistent delineation of clinically relevant regions. For ischemia assessment, oxygen saturation was estimated using a two-wavelength method, and principal component analysis combined with Gaussian mixture modeling (PCA-GMM) was applied to spectral features. The clustering revealed progressive separation of intact, moderately ischemic, and severely ischemic tissue, consistent with intraoperative surgical observations. This pipeline enables pixel-wise visualization of ischemic alterations with quantitative metrics, providing surgeons with objective and spatially resolved information to support resection decisions. The proposed framework demonstrates feasibility in clinical practice and establishes a foundation for large-scale validation and integration into intraoperative decision-support systems.

Keywords: hyperspectral imaging; intestinal ischemia; spectral clustering; convolutional neural network; tissue oxygenation; intraoperative diagnostics.

Paper #9330 received 26 Aug 2025; revised manuscript received 6 Oct 2025; accepted for publication 7 Oct 2025; published online 24 Oct 2025. doi: 10.18287/JBPE25.11.040301.

1 Introduction

Intestinal ischemia is a life-threatening surgical condition characterized by impaired blood supply to the intestinal wall, leading to necrosis and severe clinical complications if timely treatment is not provided [1]. In modern abdominal surgery, the most common method for intraoperative assessment of intestinal viability remains visual inspection and palpation, including such indicators as the color of the serosal surface, the presence and intensity of peristalsis, pulsation of marginal mesenteric vessels, and the degree of their blood filling [2, 3]. However, these criteria are largely subjective and depend on the surgeon's experience, which may result in variability of interpretation and, consequently, an increased risk of suboptimal decisions regarding the extent of resection or the preservation of potentially ischemic tissue [4].

In this regard, there is a need in clinical practice for objective and quantitative methods that allow intraoperative evaluation of the intestinal wall condition and detection of ischemic changes. Several optical approaches are already in use or are being actively developed for this purpose. The most widely applied technique is indocyanine green (ICG) fluorescence angiography, which provides real-time visualization of blood flow but requires administration of a contrast agent and is limited in penetration depth [5−7]. Diffuse reflectance spectroscopy (DRS) makes it possible to record spectral characteristics of reflected light and extract information on hemoglobin concentration and tissue oxygenation levels [8−10]. Laser speckle contrast imaging (LSCI) is used to assess microcirculation by analyzing the dynamics of speckle patterns [11, 12]. In addition, optical coherence tomography (OCT) and photoacoustic imaging are actively investigated as promising techniques for quantitative characterization of tissue status [13−16]. All these methods rely on the interaction of light with tissue to provide objective information about blood supply and oxygenation; however, they have limitations related to spatial resolution, probing depth, or the need for contrast agents.

Against this background, hyperspectral imaging (HSI) appears to be a particularly promising technology, as it combines spectral and spatial resolution, allowing analysis of reflected light across a wide wavelength range at each pixel of the image [17, 18]. This capability makes it possible to construct tissue oxygenation maps and detect ischemic changes at early stages. A number of studies have already demonstrated the feasibility of HSI for assessing intestinal viability, including in combination with machine learning methods for automatic classification and refinement of resection margins [19, 20]. However, classification models should be complemented with quantitative physiological parameters such as tissue oxygen saturation, which can be calculated from hyperspectral data and can improve the reliability of ischemia assessment [21].

2 Materials and Methods

2.1 Hyperspectral Imaging Method

For this study, a custom-developed hyperspectral imaging system was used, consisting of a broadband light source (OSL2, Thorlabs, USA) coupled to a fiber-optic ring illuminator (FRI61F50, Thorlabs, USA) and a hyperspectral camera (Specim, Spectral Imaging Ltd., Finland). The camera operated in the spectral range of 400−1000 nm with a spectral resolution of approximately 7 nm, providing 204 contiguous spectral channels and a spatial resolution of 512×512 pixels. Illumination was provided by a 50 W halogen lamp coupled into the ring light guide to ensure uniform illumination of the surgical field. The average irradiance at the tissue surface was 4 ± 0.5 mW/cm². The system was mounted on a medical stand with a reinforced articulated arm, which allowed flexible positioning of the camera above the surgical area.

During clinical procedures, hyperspectral images were recorded intraoperatively with an exposure time of 150 ms per frame. According to the protocol, hyperspectral data were obtained from 16 patients with acute abdominal pathology complicated by intestinal ischemia. In total, 16 hyperspectral cubes were collected, of which 13 were used for algorithm training, while 3 representative cases were selected for detailed demonstration of the developed approach. For calibration, a diffuse reflectance standard (fluoroplast F4 material) was applied, and all hyperspectral data were normalized to this reference using the standard formula. Prior to each measurement, the reference standard was sterilized and the optical components of the system were cleaned with alcohol wipes to comply with surgical asepsis requirements.

All clinical procedures were carried out at Orel Regional Clinical Hospital and were approved by the Ethics Committee of Orel State University (Protocol No. 2, dated September 18, 2023).

2.2 Case Report

In total, hyperspectral datasets were collected from 16 patients. For detailed illustration of the proposed pipeline, we present three representative clinical cases with different types of intestinal wall lesions. Patient 1 was a 73-year-old man diagnosed with perforated ulcer complicated by peritonitis. Patient 2 was a 66-year-old woman diagnosed with adhesive intestinal obstruction. Patient 3 was a 57-year-old man with a diagnosis of strangulated hernia. Hyperspectral arrays were recorded using the developed system for each of these patients.

3 Developed Algorithm

3.1 Data Preprocessing

Preliminary hyperspectral data processing involved several sequential steps. Initially, raw data cubes were corrected for the dark current signal by subtracting the corresponding dark reference data for both the measured and calibration cubes. Subsequently, normalization was performed relative to the diffuse reflectance standard by dividing the dark-corrected measured data by the dark-corrected calibration data. To reduce spectral noise and smooth the obtained spectra, a Savitzky-Golay filter was applied along the spectral dimension for each pixel.

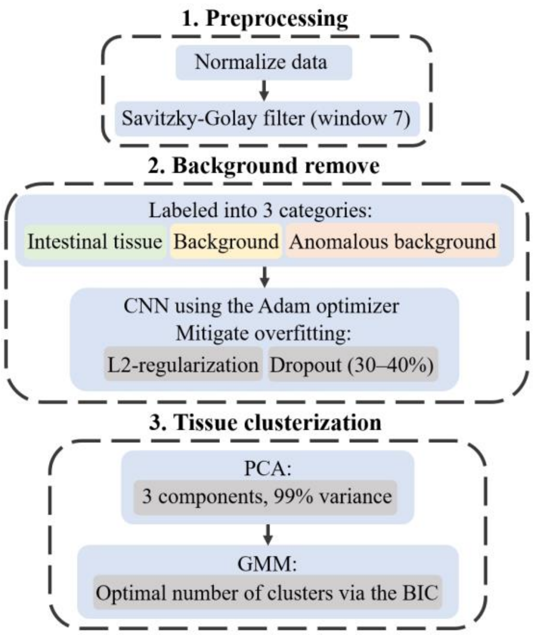

Fig. 1 Schematic representation of the data processing algorithm. The workflow includes spectral preprocessing, removal of background using CNN-based classification, and tissue clustering with PCA and GMM.

The filtered data cubes were then reshaped into a two-dimensional array suitable for subsequent machine learning-based analysis. The overall pipeline is illustrated schematically in Fig. 1.

3.2 Tissue Segmentation Using Convolutional Neural Network

Automated analysis of intraoperative hyperspectral images is complicated by multiple background elements such as surgical instruments, gauze, illumination probes, and adjacent skin, which must be differentiated from the intestinal tissues of interest. Due to the spectral complexity of these background components, conventional spectral peak analysis is insufficient. To address this, a one-dimensional convolutional neural network was designed and trained to classify individual pixel spectra independently, disregarding spatial context.

Hyperspectral cubes were manually annotated into three categories: intestinal tissue, background, and anomalous background (areas lacking proper reflectance normalization). Each pixel was represented as a one-dimensional spectral vector, yielding approximately 1.3 million spectra for training. The CNN architecture consisted of sequential convolutional layers for feature extraction, followed by fully connected layers. A sigmoid activation function was used in the output layer for binary classification. Regularization strategies included L2-penalty, dropout (30–40%), and batch normalization. Training was performed with the Adam optimizer and binary cross-entropy loss. Class imbalance was mitigated using class weighting. Early stopping and learning-rate reduction were applied to prevent overfitting.

3.3 Tissue Oxygen Saturation Estimation

Tissue oxygen saturation was estimated pixel-wise using a two-wavelength approach in the near-infrared range (750 and 795 nm), exploiting the distinct absorption of oxygenated and deoxygenated hemoglobin [22]. The algorithm was applied to intestinal regions identified by CNN-based segmentation, ensuring that background and non-relevant tissue were excluded from analysis. This approach provided spatial maps of relative oxygen saturation across the intestinal wall.

3.4 Unsupervised Spectral Analysis Using PCA-GMM

To investigate ischemic alterations without relying on histological validation or predefined labeling, an unsupervised approach was employed. Spectral data were first transformed using PCA, reducing dimensionality while retaining 99% of the variance. GMM was then applied within the PCA feature space, with the optimal number of clusters determined using the Bayesian Information Criterion (BIC).

Each hyperspectral dataset was clustered individually within the shared PCA coordinate system, ensuring comparability across cases. This framework enabled grouping of intestinal tissue spectra according to their optical characteristics.

4 Results and Discussion

The proposed approach was validated on representative intraoperative hyperspectral datasets obtained from patients with different forms and severities of intestinal pathology. The processing pipeline (Fig. 1) included CNN-based segmentation of intestinal tissue, oxygen saturation mapping, and unsupervised clustering of spectral features using PCA and GMM. Below, we present quantitative and qualitative results for each component of the pipeline and discuss their clinical interpretation.

4.1 Performance of CNN Segmentation

The one-dimensional convolutional neural network, trained on a large set of pixel spectra, demonstrated high performance in distinguishing intestinal tissue from background. On independent hyperspectral cubes not used in training, the model achieved an overall accuracy of 0.996, with precision and recall values above 0.98 and an F1-score of 0.99. These results ensured consistent identification of clinically relevant intestinal regions while reliably excluding surgical instruments, gauze, and adjacent skin. Such robust segmentation provided a stable foundation for subsequent oxygen saturation analysis and spectral clustering.

4.2 Tissue Oxygen Saturation Maps

Following segmentation, tissue oxygen saturation was estimated using the two-wavelength method (750 and 795 nm). Representative intraoperative images and corresponding saturation maps are shown in Fig. 2.

Areas of reduced oxygen saturation (blue-green regions) consistently coincided with tissue zones later assessed as ischemically compromised, whereas intact regions exhibited higher values (orange-red). This pixel-wise mapping enabled detection of localized hypoxic areas not always evident upon visual inspection and provided complementary physiological information to the surgeon's intraoperative assessment.

4.3 Spectral Clustering with PCA-GMM

Spectral vectors of the segmented intestinal tissue were projected into a PCA space retaining 99% of the original variance. GMM was then applied to identify distinct clusters, with the optimal number of components determined using the Bayesian Information Criterion. Representative results are presented in Fig. 3, where cluster maps illustrate the differentiation of intestinal tissue states. The green clusters corresponded to spectrally stable, intact tissue; the yellow clusters reflected intermediate alterations; and the red clusters indicated severe ischemic changes. Importantly, regions classified into the yellow cluster also showed reduced oxygen saturation compared to surrounding green areas, demonstrating consistency between clustering results and physiological oxygenation estimates. In the PCA feature space, clusters were clearly separated, with no overlap, confirming the robustness of spectral differentiation.

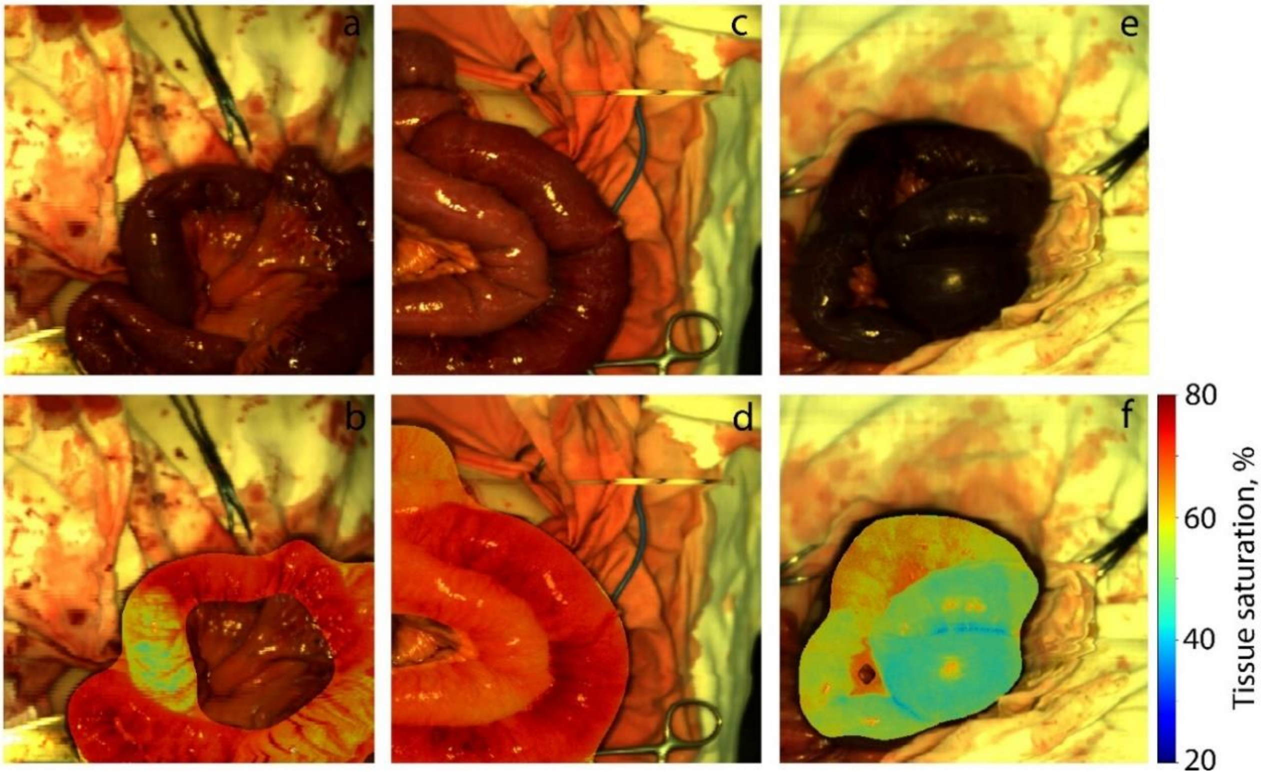

Fig. 2 Intraoperative hyperspectral imaging of the small intestine. (a, c, e) Original images recorded during surgery; (b, d, f) corresponding tissue oxygen saturation maps calculated from hyperspectral data.

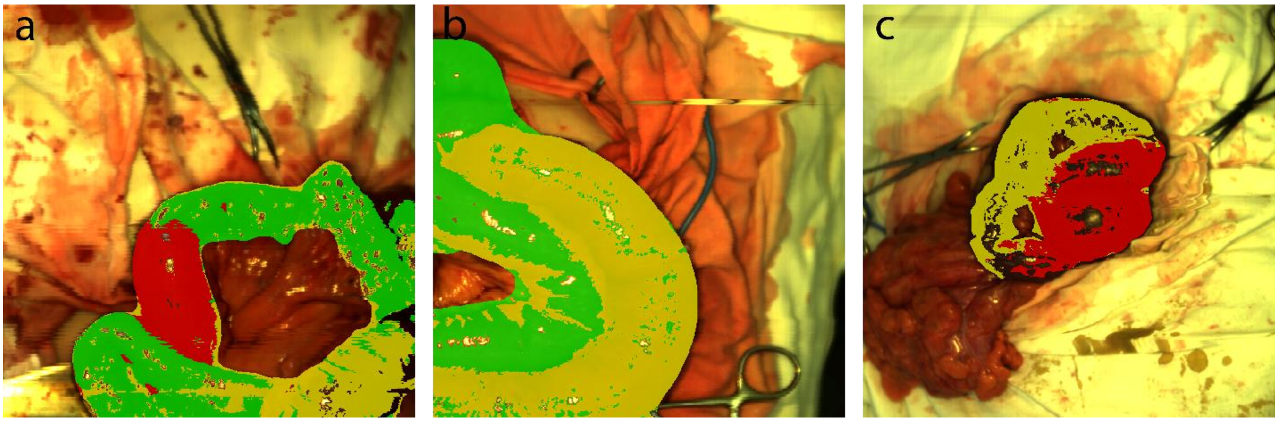

Fig. 3 Classification of intestinal tissue based on hyperspectral data. Pixel-wise cluster maps obtained using the GMM are shown for three representative cases: (a) perforated ulcer, (b) adhesive obstruction, (c) strangulated hernia. Clusters occupied distinct regions in PCA space without overlap, confirming spectral separation of tissue states.

Quantitative analysis supported these findings:

- Case (a), perforated ulcer: average saturation values were $74.0 \pm 2.1\%$ in green (intact) tissue, $68.6 \pm 3.6\%$ in yellow regions, and $61.9 \pm 5.4\%$ in red ischemic areas. These findings matched the surgeon's intraoperative assessment, where progressive ischemia surrounded the ulcerative defect.
- Case (b), adhesive obstruction: green clusters showed $70.0 \pm 2.3\%$, while yellow regions reached $74.1 \pm 2.3\%$. The paradoxically higher oxygenation in altered tissue reflected post-reperfusion measurement, when blood flow was partially restored, leading to transient hyperoxygenation.
- Case (c), strangulated hernia: yellow clusters averaged $59.2 \pm 3.2\%$, while red clusters decreased to $49.2 \pm 3.4\%$, indicating severe oxygen depletion. The clustering successfully separated the area with pronounced ischemic alterations at the hernia site from adjacent areas of progressive ischemia.

Taken together, these results demonstrate that the combined spectral-physiological analysis not only distinguished intact from ischemically altered tissue but also reflected clinically observed differences in ischemic progression across patients.

5 Conclusions

This study demonstrated the feasibility of intraoperative hyperspectral imaging for the evaluation of intestinal ischemia by integrating three analytical components: CNN-based segmentation, pixel-wise oxygen saturation mapping, and unsupervised clustering of spectral features with PCA-GMM. The combined pipeline allowed both anatomical delineation of the intestine and functional assessment of its viability.

The convolutional neural network consistently separated intestinal tissue from complex surgical backgrounds, forming a reliable basis for further analysis. Oxygen saturation maps derived from hyperspectral data highlighted localized hypoxic regions not always visible to the naked eye, providing surgeons with complementary physiological insight. Spectral clustering revealed distinct groups of tissue states – ranging from intact to progressively ischemic and severely altered – that correlated with intraoperative observations and demonstrated meaningful differences in tissue oxygenation levels. By combining anatomical, physiological, and spectral information, the proposed approach revealed a continuous transition from viable to severely altered tissue, reflecting the progressive nature of ischemic injury. This integrative framework can be applied to new clinical data, offering a pathway toward scalable validation, standardization of spectral features, and eventual incorporation into intraoperative decision-support systems for improved surgical outcomes.

Disclosures

The authors declare no conflicts of interest in this paper.

Acknowledgements

This work was supported by a grant from the Russian Science Foundation (No. 25-25-00482).

References

1. D. G. Clair, J. M. Beach, "Mesenteric ischemia," New England Journal of Medicine 374(10), 959−968 (2016).
2. G. Lu, B. Fei, "Medical hyperspectral imaging: a review," Journal of Biomedical Optics 19(1), 010901 (2014).
3. L. Urbanavičius, P. Pattyn, D. Van de Putte, and D. Venskutonis, "How to assess intestinal viability during surgery: a review of techniques," World Journal of Gastrointestinal Surgery 3(5), 59−69 (2011).
4. N. A. Adamenkov, A. Mamoshin, V. Dremin, E. Potapova, V. Shupletsov, I. Gotyunov, A. Palalov, and A. Dunaev, "Assessment of intestinal wall perfusion under ischemic conditions using hyperspectral imaging," Russian Journal of Operative Surgery and Clinical Anatomy 8(1), 5−13 (2024). [in Russian]
5. T. Degett, H. S. Andersen, and I. Gögenur, "Indocyanine green fluorescence angiography for intraoperative assessment of gastrointestinal anastomotic perfusion: a systematic review of clinical trials," Langenbeck's Archives of Surgery 401(6), 767–775 (2016).
6. P. D. McEntee, A. Singaravelu, C. A. McCarrick, E. Murphy, P. A. Boland, and R. A. Cahill, "Quantification of indocyanine green fluorescence angiography in colorectal surgery: a systematic review of the literature," Surgical Endoscopy 39(4), 2677–2691 (2025).
7. G. Tang, D. Du, J. Tao, and Z. Wei, "Effect of indocyanine green fluorescence angiography on anastomotic leakage in patients undergoing colorectal surgery: a meta-analysis of randomized controlled trials and propensity-score-matched studies," Frontiers in Surgery 9, 815753 (2022).
8. J. Hou, S. S. Ness, J. Tschudi, M. O'Farrell, R. Veddegjerde, Ø. G. Martinsen, T. I. Tønnessen, and R. Strand-Amundsen, "Assessment of intestinal ischemia–reperfusion injury using diffuse reflectance VIS-NIR spectroscopy and histology," Sensors 22(23), 9111 (2022).
9. B. R. Karakaş, A. Sırcan-Küçüksayan, Ö. G. Elpek, and M. Canpolat, "Investigating viability of intestine using spectroscopy: a pilot study," Journal of Surgical Research 192(1), 91–98 (2014).
10. B. Yu, H. L. Fu, and N. Ramanujam, "Instrument independent diffuse reflectance spectroscopy," Journal of Biomedical Optics 16(1), 011010 (2011).
11. R. Paramasivam, N. M. Kristensen, R. Ambrus, M. Stavsetra, M.-B. Ørntoft, and A. Husted Madsen, "Laser speckle contrast imaging for intraoperative assessment of intestinal microcirculation in normo- and hypovolemic circulation in a porcine model," European Surgical Research 65(1), 1–8 (2024).
12. D. J. I. Heuvelings, M. Al-Taher, J. Calon, M. Chand, L. P. S. Stassen, T. Lubbers, K. P. Wevers, L. Boni, N. D. Bouvy, and W. Heeman, "Real-time intestinal perfusion assessment for anastomotic site selection using laser speckle contrast imaging: verification in a porcine model," Surgery Open Science 26, 12–17 (2025).
13. E. B. Kiseleva, M. Ryabkov, M. Baleev, E. Bederina, P. Shilyagin, A. Moiseev, V. Beschastnov, I. Romanov, G. Gelikonov, and N. Gladkova, "Prospects of intraoperative multimodal OCT application in patients with acute mesenteric ischemia," Diagnostics 11(4), 705 (2021).
14. C. Jelly, J. Kwun, R. Schmitz, A. B. Farris, Z. A. Steelman, D. L. Sudan, S. J. Knechtle, and A. P. Wax, "Optical coherence tomography of small intestine allograft biopsies using a handheld surgical probe," Journal of Biomedical Optics 26(9), 096008 (2021).

15. R. Wang, T. Pan, L. Huang, C. Liao, Q. Li, H. Jiang, and J. Yang, "Photoacoustic imaging in evaluating early intestinal ischemia injury and reperfusion injury in rat models," Quantitative Imaging in Medicine and Surgery 11(7), 2968–2979 (2021).
16. H. Yan, Z. Gou, H. Wang, X. Zhu, J. Liu, W. Ling, L. Huang, and Y. Luo, "Photoacoustic oxygenation imaging to identify ischemia/hypoxia injury and necrosis of intestine after acute intussusception: a comparative study with CDFI/CEUS," Photoacoustics 43, 100706 (2025).
17. E. Zherebtsov, V. Dremin, A. Popov, A. Doronin, D. Kurakina, M. Kirillin, I. Meglinski, and A. Bykov, "Hyperspectral imaging of human skin aided by artificial neural networks," Biomedical Optics Express 10(7), 3545 (2019).
18. V. Dremin, Z. Marcinkevics, E. Zherebtsov, A. Popov, A. Grabovskis, H. Kronberga, K. Geldnere, A. Doronin, I. Meglinski, and A. Bykov, "Skin complications of diabetes mellitus revealed by polarized hyperspectral imaging and machine learning," IEEE Transactions on Medical Imaging 40(4), 1207–1216 (2021).
19. L. Zhang, D. Huang, X. Chen, L. Zhu, Z. Xie, X. Chen, G. Cui, Y. Zhou, G. Huang, and W. Shi, "Discrimination between normal and necrotic small intestinal tissue using hyperspectral imaging and unsupervised classification," Journal of Biophotonics 16(7), e202300020 (2023).
20. L. Zhang, Y. Zhou, D. Huang, L. Zhu, X. Chen, Z. Xie, G. Cui, G. Huang, S. Ali, and X. Chen, "Hyperspectral imaging combined with deep learning to detect ischemic necrosis in small intestinal tissue," Photonics 10(7), 708 (2023).
21. N. Gustafsson, J. Bunke, L. Magnusson, J. Albinsson, J. Hernandez-Palacios, R. Sheikh, M. Malmsjö, and A. Merdasa, "Optimizing clinical O_2 saturation mapping using hyperspectral imaging and diffuse reflectance spectroscopy in the context of epinephrine injection," Biomedical Optics Express 15(3), 1995−2013 (2024).
22. E. V. Potapova, V. V. Dremin, E. A. Zherebtsov, I. N. Makovik, A. I. Zherebtsova, A. V. Dunaev, K. V. Podmasteryev, V. V. Sidorov, A. I. Krupatkin, L. S. Khakhicheva, and V. F. Muradyan, "Evaluation of microcirculatory disturbances in patients with rheumatic diseases by the method of diffuse reflectance spectroscopy," Human Physiology 43(2), 222−228 (2017).